ACS APPLIED MATERIALS & INTERFACES

Research Article

www.acsami.org

Magnetism-Driven Ferroelectricity in Double Perovskite Y_2NiMnO_6

J. Su,*[,†,§] Z. Z. Yang,[‡] X. M. Lu,*[,§] J. T. Zhang,[§] L. Gu,*[,‡] C. J. Lu,[†] Q. C. Li,[†] J.-M. Liu,[§] and J. S. Zhu[§]

[†]College of Physics Science, Key Laboratory of Photonics Materials and Technology in Universities of Shandong, Qingdao University, Ningxia Road, Qingdao Shinan District No. 22, Qingdao 266071, China

[‡]Beijing National Laboratory for Condensed Matter Physics, Institute of Physics, Chinese Academy of Sciences, Beijing 100190, China

[§]National Laboratory of Solid State Microstructures, Physics School, Nanjing University, Nanjing 210093, China

ABSTRACT: We report the discovery of multiferroic behavior in double perovskite Y_2NiMnO_6. X-ray diffraction shows that the material has a centrosymmetric crystal structure of space group $P2_1/n$ with Ni^{2+}/Mn^{4+} ordering. This result is further confirmed by aberration-corrected scanning transmission electron microscopy combined with atomic resolution electron energy loss spectroscopy. The appearance of ferroelectric polarization coincides with the magnetic phase transition (~67 K), which indicates that the ferroelectricity is driven by magnetism, and this is further confirmed by its strong magnetoelectric (ME) effect. We proposed the origin of the ferroelectricity is associated with the combination of Ni^{2+}/Mn^{4+} charge ordering and the ↑↑↓↓ spin ordering. When compared with other known magnetic multiferroics, Y_2NiMnO_6 displays several attractive multiferroic properties, including high polarization (~145 $\mu C/m^2$), a high multiferroic transition temperature (~67 K), and strong ME coupling (~21%).

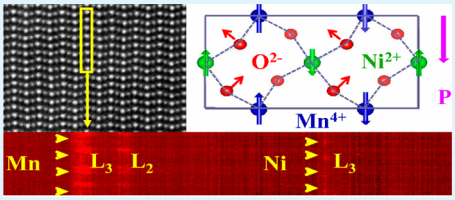

KEYWORDS: *Y_2NiMnO_6, sol–gel, STEM, multiferroics, magnetoelectric effect*

1. INTRODUCTION

Materials with coexisting magnetic and ferroelectric orders, known as multiferroics, are attracting enormous scientific interest because of their potential applications to sensors, novel circuits, storage devices, and microwave technology.[1−3] To avoid the natural exclusion between magnetism and ferroelectricity, several routes can be used to obtain multiferroicity.[4] Depending on the origin of the polarization of the material, multiferroics can be classified into two families.[5] Type-1 multiferroics, where the magnetism and the ferroelectricity have different origins, often present high polarizations and high critical temperatures. In contrast, type-2 multiferroics (i.e., magnetic multiferroics), where the ferroelectricity is caused by an exotic magnetic order rather than by a noncentrosymmetric crystal structure, are more interesting and important because both orders tend to be strongly coupled.[6] However, current type-2 multiferroics have two important drawbacks: low critical temperatures (T_c) and low polarization (P) values. To overcome these problems, considerable effort has recently focused on the design of new magnetic multiferroics. One confirmed example involves the collinear magnetic structured manganite Ca_3CoMnO_6, which has a relatively high polarization (~400 $\mu C/m^2$).[7] In Ca_3CoMnO_6, the Co^{2+} ions and Mn^{4+} ions are distributed alternately along the c-axis, i.e., they produce Co^{2+}/Mn^{4+} ionic (charge) ordering and form a ↑↑↓↓ spin order, which breaks the inversion symmetry on the magnetic sites along the chain and can induce electric polarization along the chain via exchange striction.[7,8] Magnetostriction-driven ferroelectricity induced by collinear magnetic ordering is specifically applicable to double perovskite manganites with the formula $A_2BB'O_6$. The ferroelectric T_c of double perovskite manganites is considerably higher than that of typical magnetic multiferroics. For example, the T_c of Y_2CoMnO_6 is 80 K,[9] which is above liquid nitrogen temperature, while the corresponding values for $ReMnO_3$ (where Re = Lu, Tm, Ho, Y, Dy, Tb) are all below 35 K.[10] At present, these double perovskites are considered promising candidates for large P, high T_c, and strong magnetoelectric (ME) coupling materials.[9] First-principles density functional theory shows that the magnetic order in double perovskite manganites of the form Re_2NiMnO_6 (where Re = La, Sm, and Y) changes from ferromagnetic (for Re = La and Sm) to E-type when Re = Y.[11] In addition, a ferroelectric polarization can be induced by this E-type magnetism because of a break in the inversion symmetry, and the predicted P of Y_2NiMnO_6 is ~2500 $\mu C/m^2$,[11] which is comparable with the spontaneous polarization of ferroelectric materials (e.g., ~15000 $\mu C/m^2$ in $BaTiO_3$[12]). However, so far, there have been few detailed experiments concerning this prediction, especially on ME coupling.

In addition, a well-defined B/B′ ionic order is a prerequisite for multiferroicity in double perovskites. Thus, investigation of the distributions of B and B′ ions in double perovskites is of considerable interest from the viewpoints of both the fundamental physics and potential applications. However, it is very difficult to detect the distributions of ions with atomic

Received: January 30, 2015
Accepted: May 27, 2015
Published: May 27, 2015

DOI: 10.1021/acsami.5b00911
ACS Appl. Mater. Interfaces 2015, 7, 13260−13265

numbers that are very similar by using traditional techniques such as X-ray diffraction (XRD) because of the reduced contrast among the scattering intensities of these ions, which constrains all octahedral sites to equivalence.[13−16] Therefore, a method that allows direct mapping of the distributions and the valence states of B and B′ ions in double perovskites at atomic resolution should provide greater insight into the origin of the multiferroicity. Recent technological breakthroughs in electron spectromicroscopy techniques have paved the way toward localization of the single atom positions and acquisition of 2D elemental maps of large unit cells with subangstrom resolution.[16−19] Aberration-corrected scanning transmission electron microscopy (STEM) combined with atomic resolution electron energy loss spectroscopy (EELS) can probe the electronic structures and the local bonding environments of these functional materials.[20,21]

Here, we present results for Y_2NiMnO_6, in which the net electric polarization and the net magnetization coexist and couple at temperatures below 67 K. The magnetic orderings have frustrated Ising spin chains with ↑↑↓↓ spin patterns, which break the spatial inversion symmetry and in turn lead to the emergence of ferroelectricity. Our results for Y_2NiMnO_6 therefore bring us one step closer to operation at practical temperatures and suggest that an ↑↑↓↓ magnetic structure coupled to ferroelectricity can be a widespread ME-coupling mechanism. In addition, we highlight direct Ni^{2+}/Mn^{4+} charge ordering experiments using an atomically resolved real space spectroscopy technique, i.e., aberration-corrected STEM-EELS.

2. EXPERIMENTAL SECTION

Polycrystalline Y_2NiMnO_6 powder was prepared by the sol−gel method. AR (analytical reagent) grade $Y(NO_3)_3{\cdot}6H_2O$ (4N purity), $Ni(NO_3)_3{\cdot}6H_2O$ (3N purity), and $C_4H_6MnO_4{\cdot}6H_2O$ (3N purity) were dissolved in equal weights of distilled water according to their stoichiometric ratios. An appropriate amount of citric acid was added while stirring continuously, and the molar ratio of the citric acid to the total number of metal ions was maintained at 2:1. The solvent was evaporated directly at 150 °C until a thick sol was formed, and this sol was then preheated at 1000 °C for 12 h. The powder obtained was then milled with ∼0.1 wt % poly(vinyl alcohol) added as a binder and was pressed into pellets with diameters of 12 mm and thicknesses of 2−3 mm under uniaxial pressure of 40 MPa. A dense Y_2NiMnO_6 ceramic was obtained by sintering at 1260 °C for 20 h at a heating rate of 6 °C/min and then allowing the ceramic to cool naturally. An X-ray diffractometer (XRD, Bruker D8) with Cu Kα radiation (λ = 1.5418 Å) and aberration-corrected STEM (JEM ARM200F, JEOL) equipped with an atomic resolution electron energy loss spectroscopy (EELS) system were used to analyze the microstructure. The combination states of Mn 2p and Ni 2p electrons in Y_2NiMnO_6 were measured by X-ray photoelectron spectroscopy (XPS, ESCALAB 250). The magnetic properties of the sample were examined using a magnetic properties measurement system (MPMS-7, Quantum Design). With Pt pastes deposited on the sample surface acting as electrodes, the dielectric constant and P were measured using a physical properties measurement system (PPMS-7, Quantum Design). P was obtained by integrating the pyroelectric current that was measured using the Keithley 6514A during the warming process without any electrical bias, while the samples were poled under an electric field E = 3.6 kV/cm during the cooling process. The details of the measurement processes can be found in our previous reports.[22,23]

3. RESULTS AND DISCUSSION

Figure 1a presents the XRD pattern and Rietveld refinement profile of Y_2NiMnO_6 powder. The XRD results show that it has a single phase, and no impurity phase is present. The crystal

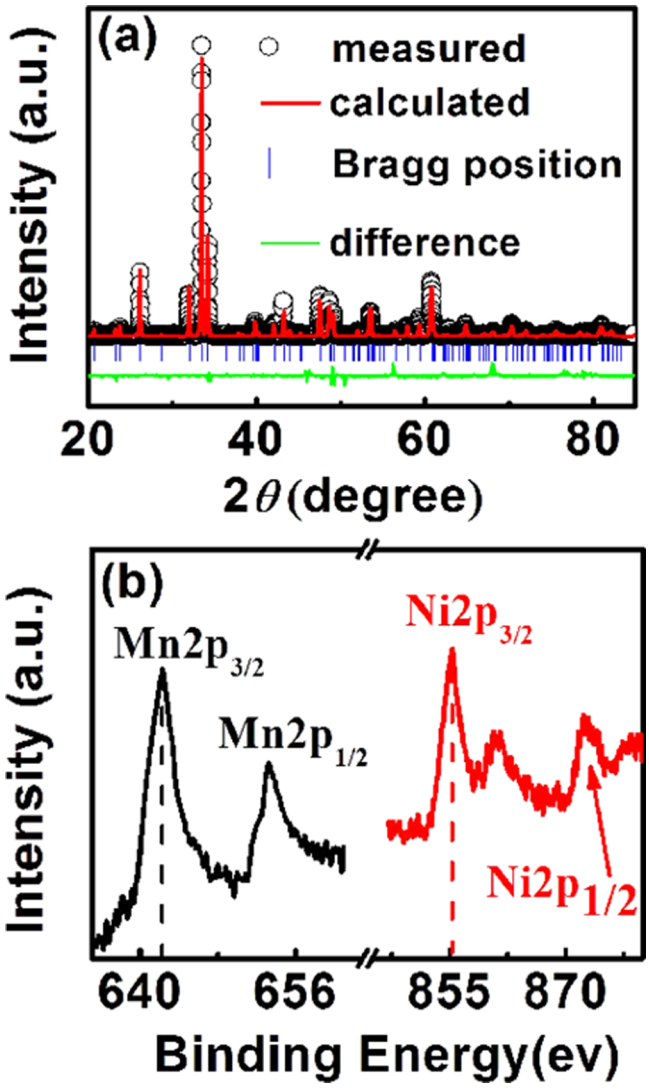

Figure 1. (a) Results of Rietveld refinement analysis of the XRD pattern. Red solid lines, black open circles, and green solid lines show the calculated, experimental, and difference patterns, respectively. The Bragg peak positions are marked by blue sticks. (b) XPS spectrum of the Mn 2p and (Left) and Ni 2p regions (right) of Y_2NiMnO_6.

structure with a monoclinic $P2_1/n$ space group was refined from Rietveld analysis using the GSAS/EXPGUI system.[24] The difference between the refined spectrum and the measured one is very small. The reliability is ensured by the Rietveld refinement parameter R_{Wp} = 7.66% with lattice parameters a = 5.2212 Å, b = 5.5212 Å, c = 7.4803 Å, and β = 89.8213°. The XPS spectrum was used to investigate the valencies of Mn and Ni ions in Y_2NiMnO_6. Figure 1b depicts the XPS spectrum of the Mn 2p and Ni 2p region. The results show that the peak of Mn $2P_{3/2}$ is ∼642.3 eV. Because the $2P_{3/2}$ core level appears at 642.4 and 641.8 eV for Mn^{4+} and Mn^{3+}, respectively, our data reveal with certainty that the valence of Mn is +4 in our sample.[25] The peak of Ni $2P_{3/2}$ is ∼855.5 eV, in agreement with the value (855.4 eV) reported for Ni^{2+},[26] indicating that the valence of Ni is +2 in Y_2NiMnO_6 ceramics.

To date, the study of the distributions of the B and B′ ions in double perovskite structures has primarily depended on XRD and neutron diffraction techniques. Here, aberration-corrected STEM-EELS was used to directly investigate the distributions of the Ni^{2+} and Mn^{4+} ions in Y_2NiMnO_6 ceramics. Figure 2a

DOI: 10.1021/acsami.5b00911
ACS Appl. Mater. Interfaces 2015, 7, 13260−13265

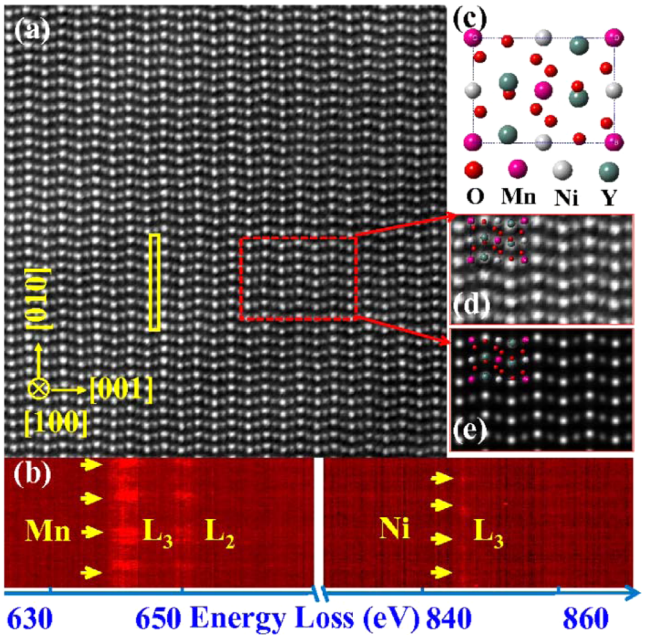

Figure 2. STEM images of the Y_2NiMnO_6 structure. (a) HAADF image. (b) Atomic scale STEM-EELS line scanning spectra corresponding to the yellow-framed area in (a). (c) Crystal structure viewed along the [100] direction. (d) Enlarged view of the red dotted framed area in (a). (e) Simulated HAADF image corresponding to (d).

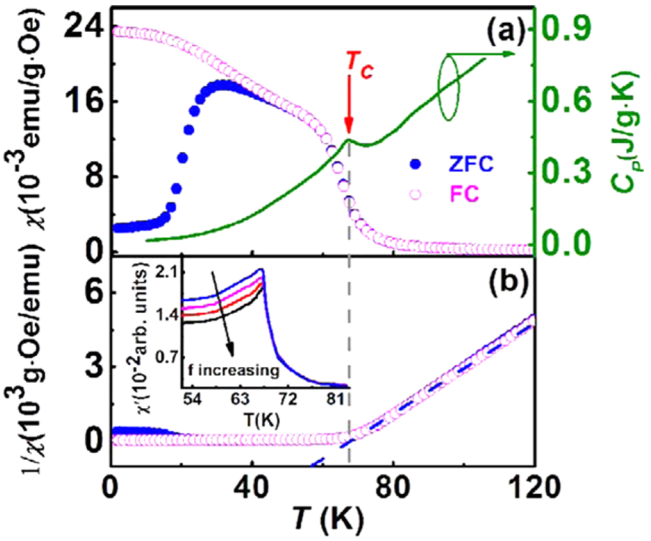

Figure 3. (a) DC magnetic susceptibility (χ, for FC and ZFC) and specific heat (C_p) vs T. (b) Inverse susceptibility ($1/\chi$) vs T. The inset of (b) shows the AC susceptibility (χ') vs T at various frequencies.

shows a high annular dark field (HAADF)-STEM image of Y_2NiMnO_6 ceramics. The Y^{3+} column and the Ni^{2+} (Mn^{4+}) column can be clearly distinguished because of their strong atomic number (Z) differences; however, it is difficult to distinguish directly between the Ni^{2+} column and the Mn^{4+} column because there is no significant Z difference between them. Therefore, EELS with an energy resolution of 0.4 eV was used to demonstrate the distributions of the Ni^{2+} and Mn^{4+} ions; the Mn $L_{2,3}$ and Ni L_3 edges were acquired simultaneously with an energy dispersion of 0.25 eV/pixel. The results, which correspond to the yellow rectangular framed area in Figure 2a, are shown in Figure 2b. As indicated by the marked arrows, it can be seen clearly that the Ni^{2+} column and the Mn^{4+} column are distributed alternately, i.e., they show Ni^{2+}/Mn^{4+} ion ordering. Figure 2d shows an enlarged view of the red dotted frame area in Figure 2a, and it can be seen that it matches the crystal structure of Y_2NiMnO_6 with space group $P2_1/n$ well (Figure 2c). In addition, the results were simulated with the STEMSIM software package;[27] the simulated map is shown in Figure 2e and matches the measured maps well in terms of both position and column contrast, which further confirms the Ni^{2+}/Mn^{4+} ordering in Y_2NiMnO_6. To determine whether the Ni^{2+}/Mn^{4+} ion ordering occurs throughout the whole sample, we investigated different regions of the sample, and the results show that the degree of order almost approaches a fully ordered state.

First, we consider the magnetic properties. Figure 3a shows the thermal variation in the DC magnetic susceptibility (χ) of Y_2NiMnO_6 in the 2−100 K temperature range, with zero field cooling (ZFC) and field cooling (FC). The specific heat (C_p) of the sample is also shown in Figure 3a in the 15−95 K range. Spontaneous magnetization begins to develop at T_c = 67 K. The Curie−Weiss law [$\chi = C/(T - \theta_{CW})$] is used to fit the data above ~67 K, and good paramagnetic behavior is observed above T_c (Figure 3b). The extrapolated temperature θ_{CW} is ~57.6 K, which implies that a ferromagnetic interaction occurs below T_c.[28] The phase transition at T_c was further confirmed by C_p, which showed a sharp anomaly at this temperature. As previously mentioned, the magnetic structure was considered to be E-type antiferromagnetic with ↑↑↓↓ spin structure.[11] However, the magnetic data presented here surprisingly displays characteristics of a ferromagnet. The contradiction between these results may be explained by the following analysis. The neutron diffraction measurement confirmed Lu_2CoMnO_6 has the same ↑↑↓↓ spin structure,[29] while magnetic hysteresis curves display ferromagnetic character, which were very similar to our results. The experimental results of Lu_2CoMnO_6 show that the ↑↑↓↓ spin structure was only taken in zero magnetic field and can be destroyed when measured magnetic fields were applied. On the basis of above results, we propose that the ↑↑↓↓ spin structure of Y_2NiMnO_6 can be transformed into ferromagnetic under applied magnetic fields, which can explain the puzzle about the presence of ferroelectricity and the ferromagnetic hysteresis curve. As for the magnetic susceptibility results, positive θ_{CW} obtained by Curie−Weiss law fitting indicates the ferromagnetic nearest-neighbor exchange interaction, which does not contradict with the ↑↑↓↓ spin structure, the theoretical studies have shown that the ↑↑↓↓ spin structure common originates from the competition between nearest-neighbor and next-nearest-neighbor exchange interactions, such as Ca_3CoMnO_6 and $RMnO_3$ with E-type order.[7,8,11] In the inset of Figure 3b, we show the temperature dependence of the AC susceptibility (χ') at ~1, 10, 100, and 1000 Hz. Long-range magnetic ordering is clearly demarcated near 67 K, below which frequency-dependent characteristics are observed. This behavior is caused by the movement of domain walls, which is an efficient means of controlling the ferroelectric polarization using a magnetic field and involving magnetostriction.[9,29] Although $M-H$ hysteresis results are not presented here, hysteresis plots with a coactivity of ~0.27 T (at 2 K) were obtained that showed an unsaturated moment of ~3.9 μ_B per formula up to 6 T. This value is close to the 5 μ_B per formula expected from Ni^{2+} (S = 1) and Mn^{4+} (S = 3/2)[28] but is still smaller, which may be

DOI: 10.1021/acsami.5b00911
ACS Appl. Mater. Interfaces 2015, 7, 13260−13265

caused by the weak measured magnetic field. A similar phenomenon was also observed by Yáñez-Vilar et al. in Lu_2CoMnO_6 ceramics.[29] They found that the magnetization is ~4.5 μ_B per formula at 13 T. The expected full moment of 6 μ_B per formula is only achieved at a strong pulse magnetic field of 60 T.[29]

To investigate the ferroelectric properties, the dielectric constant (ε) was measured as a function of temperature (T) at a frequency of 1 kHz, as shown in Figure 4a. A small but clear

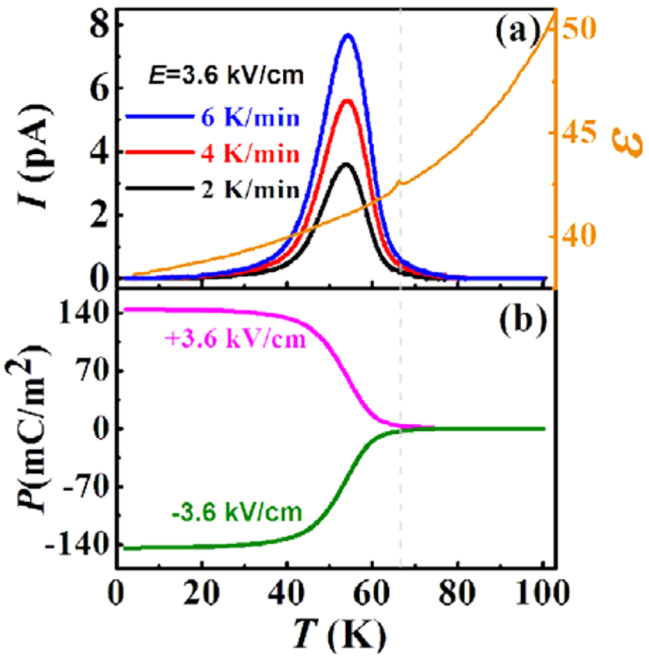

Figure 4. (a) Pyroelectric currents for various warming rates (I) and the dielectric constant (ε) vs T. (b) The (symmetric) ferroelectric polarizations under positive and negative poling electric fields.

anomaly in the $\varepsilon-T$ curve is identified at 67 K, indicating a ferroelectric transition that coincides with T_c, the ferromagnetic transition point. More interestingly, a ferroelectric transition emerges at this ferromagnetic transition point, which suggests the presence of ferroelectricity driven by magnetism. In other words, Y_2NiMnO_6 is shown here to be a ferromagnetic multiferroic material. The reliability of the measured $P(T)$ is proved using the pyroelectric current (I) as a function of temperature (T) with various warming rates (2, 4, and 6 K/min), as depicted in Figure 4a. The peaks of the $I-T$ curves do not shift along the T-axis, and the integrals of $I(t)$ of each of the curves are almost identical, indicating that error sources such as mobile charged defects or thermally stimulated currents, if they exist, do not contribute appreciably to the measured $I(t)$; thus, the intrinsic $I(t)$ is dominant. We also measured $P(T)$ under positive and negative poling electric fields of $E = \pm 3.6$ kV/cm. The polarity of P is determined by the sign of E, as shown in Figure 4b, thus confirming the genuine ferroelectricity in Y_2NiMnO_6. Under the poling field of $E = 3.6$ kV/cm, the measured P is as high as ~145 $\mu C/m^2$ under a zero external magnetic field. When compared with other magnetic multiferroics, the multiferroicity of Y_2NiMnO_6 is remarkable. First, the ferroelectric T_c is considerably higher than that of other known multiferroics with ↑↑↓↓ magnetic structures. For example, the T_c values of Ca_3CoMnO_6 and Lu_2CoMnO_6 are 14 and 35 K, respectively.[9,28] Second, the observed P (~145 $\mu C/m^2$) is high when the polycrystalline nature of the sample and its small crystal grains are considered. For Ca_3MnCoO_6 ceramics, which also have polarization induced by exchange striction, P is approximately 1/138 of the single crystal value.[7,8] Therefore, if a single crystal of Y_2NiMnO_6 was synthesized, the expected P would be ~20 mC/m^2, which is comparable with the spontaneous polarization of ferroelectric materials.

In addition, the existence of magnetically induced ferroelectricity was further confirmed by the presence of a strong ME effect, as indicated by the magnetic field (H) dependence of P. During the measurements, the sample is cooled from 100 to 2 K under various values of H and using a fixed $E = 3.6$ kV/cm. As shown in Figure 5a, the measured P is suppressed by the

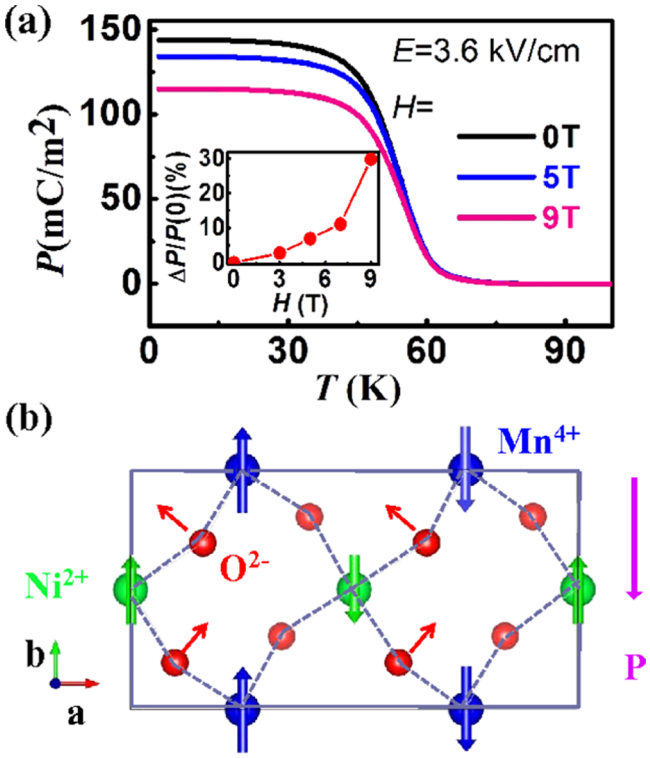

Figure 5. (a) Suppression of the ferroelectric polarization (P) by a magnetic field. The inset of (a) depicts the magnetoelectric (ME) response ratio under various magnetic field (H) conditions. (b) The diagrammatic sketch of symmetrical exchange-striction mechanism present in Y_2NiMnO_6 with ↑↑↓↓ spin order. The thin red arrows denote the displacement of O^{2-} ions caused by the nonequivalent exchange interactions, and the long purple arrow denotes the total ferroelectric polarization direction.

applied H, e.g., P decreases from 145 to 114 $\mu C/m^2$ at 2 K under a field of $H = 9$ T, while T_c is almost unchanged, which indicates a robust magnetic transition. The ME effect, which is defined as $[P(0) - P(H)]/P(0) \times 100\%$, is as high as 21% when $H = 9$ T, as shown in the inset of Figure 5a. When the polycrystalline nature of the sample is considered, this ME effect is large and implies the presence of magnetism-driven ferroelectricity inY_2NiMnO_6.

The large P originates from the exchange striction interactions under the ↑↑↓↓ spin structure, in which the microscopic mechanism is similar to $RMnO_3$ with E-type order, as has been shown in Figure 5b. Because of the nearest-neighbor ferromagnetic exchange interaction,[8,11] the nonequivalent exchange interactions of adjacent spin pairs would

DOI: 10.1021/acsami.5b00911
ACS Appl. Mater. Interfaces 2015, 7, 13260−13265

cause the displacements of O^{2-} ions. The O^{2-} ions connecting parallel spins would move along the direction of perpendicular to the bond to increase the bond angles, and the O^{2-} ions connecting antiparallel spins would move to decrease the bond angle. This would induce macroscopic ferroelectric polarization perpendicular to the wave vector of ↑↑↓↓ spin order. This kind of symmetric polarization is also observed in Lu_2CoMnO_6, and Y_2CoMnO_6.[9,29] Recently, Maiti et al. fabricated nanocrystalline Y_2NiMnO_6;[30] however, the ferroelectric transition is far above the magnetic transition, which is probably caused by chemical inhomogeneity or the coexistence of Mn^{3+} and Mn^{4+}.[26] The ferroelectricity of Y_2NiMnO_6 was also investigated by Zhang et al. using the PUND model,[26] but the value of P is only ∼30 $\mu C/m^2$, about a fifth of ours (∼145 $\mu C/m^2$). The small value is probably due to the measured temperature (77 K), which is only 7 K lower than the Curie temperature (84 K), because the P will decrease rapidly with increasing temperature near the Curie temperature, especially for type II multiferroics. Furthermore, the ME coupling is one of the most important property of multiferroics with respect to the possibility to control electric properties by a magnetic field and vice versa. However, neither of these studies investigated the ME coupling in Y_2NiMnO_6.

According to the experimental results and above analysis, a sufficiently large magnetic field can induce the transition from ↑↑↓↓ spin order to the ferromagnetic order. The electric polarization can be destroyed along with the transition process, which produces the observed ME coupling.[7−9,29] The results and the mechanism are similar to that in Ca_3CoMnO_6,[7,8] with the difference in Ca_3CoMnO_6 being that the measured P decreases rapidly with increasing T, rather than the situation in Y_2NiMnO_6, where the measured P shows little change with increasing T. The difference between these material characteristics may be ascribed to the fact that the interchain interactions on the $a-b$ plane in Ca_3CoMnO_6 are weaker than those in Y_2NiMnO_6.[31,32] It should be noted here that the spin order of Y_2NiMnO_6 under magnetic fieldmay be very complex. Therefore, further research is required to confirm the proposed mechanism for the observed multiferroicity here.

4. CONCLUSION

Y_2NiMnO_6 ceramics with double perovskite structures were prepared by the sol−gel method. We have shown that Y_2NiMnO_6 is a new member of the group of magnetism-driven ferroelectric materials. XRD, XPS, and STEM-EELS confirmed that the material has a centrosymmetric crystal structure of space group $P2_1/n$ with Ni^{2+}/Mn^{4+} ordering at room temperature. The multiferroic properties of the material are attractive (large P, high T_c, and strong magnetoelectric response) when compared with those of other known multiferroic manganites. The exchange striction mechanism under ↑↑↓↓ spin configuration and Ni^{2+}/Mn^{4+} charge ordering conditions is considered to be the driving force behind the emergence of the ferroelectricity.

AUTHOR INFORMATION

Corresponding Authors

*For J.S.: E-mail, jsu@qdu.edu.cn.
*For L.G.: E-mail, gu@iphy.ac.cn.
*For X.M.L.: E-mail, xiaomeil@nju.edu.cn.

Author Contributions

J.S. and Z.Z.Y. contributed equally to this work.

Notes

The authors declare no competing financial interest.

ACKNOWLEDGMENTS

This work was supported by the State Key Program for Basic Researches of China (nos. 2014CB921002 and 2009CB929501), National Science Foundation of China (nos. 11374169, 51472131, 61271078, 51225201, and 11174166), the Distinguished Middle-aged and Young Scientist Encourage and Reward Foundation of Shandong Province, China (nos. BS2013CL006 and BS2014BSB1032), the Strategic Priority Research Program of the Chinese Academy of Sciences (grant no. XDB07030200), the Fundamental Research Funds for the Central Universities, the Priority Academic Program Development of Jiangsu Higher Education Institutions, and open project of National Laboratory of Solid State Microstructures (M27003).

REFERENCES

(1) Ramash, R.; Spaldin, N. Multiferroics: Progress and Prospects in Thin Films. *Nature Mater.* **2007**, *6*, 21−29.
(2) Lottermoser, T.; Mathur, N. D.; Scott, J. F. Multiferroic and Magnetoelectric Materials. *Nature* **2006**, *442*, 759−765.
(3) Jiang, K.; Zhu, J. J.; Wu, J. D.; Sun, J.; Hu, Z. G. Influences of Oxygen Pressure on Optical Properties and Interband Electronic Transitions in Multiferroic Bismuth Ferrite Nanocrystalline Films Grown by Pulsed Laser Deposition. *ACS Appl. Mater. Interfaces* **2011**, *3*, 4844−4582.
(4) Hill, N. A. Why Are There So Few Magnetic Ferroelectrics? *J. Phys. Chem. B* **2000**, *104*, 6694−6709.
(5) Khomskii, D. Trend: Classifying Multiferroics: Mechanisms and Effects. *Physics* **2009**, *2*, 20−27.
(6) Zhang, G. Q.; Dong, S.; Yan, Z. B.; Zhang, Q. F.; Yunoki, S. J.; Dagotto, E.; Liu, J.-M. Multiferroic Properties of $CaMn_7O_{12}$. *Phys. Rev. B* **2011**, *84*, 174413−174417.
(7) Jo, Y. J.; Lee, S.; Choi, E. S.; Yi, H. T.; Ratcliff, W.; Choi, Y. J.; Kiryukhin, V.; Cheone, S. W.; Balicas, L. 3:1 Magnetization Plateau and Suppression of Ferroelectric Polarization in an Ising Chain Multiferroic. *Phys. Rev. B* **2009**, *79*, 012407−012410.
(8) Choi, Y. J.; Yi, H. T.; Lee, S.; Huang, Q.; Kiryukhin, V.; Cheong, S.-W. Ferroelectricity in an Ising Chain Magnet. *Phys. Rev. Lett.* **2008**, *100*, 047601−047604.
(9) Sharma, G.; Saha, J.; Kaushik, S. D.; Siruguri, V.; Patnaik, S. Magnetism Driven Ferroelectricity Above Liquid Nitrogen Temperature in Y_2CoMnO_6. *Appl. Phys. Lett.* **2013**, *103*, 012903−012906.
(10) Ishiwata, S.; Kaneko, Y.; Tokunaga, Y.; Taguchi, Y.; Arima, T. K.; Tokuta, Y. Perovskite Manganites Hosting Versatile Multeferroic Phases with Symmetric and Antisymmetric Exchange Strictions. *Phys. Rev. B* **2010**, *81*, 100411(R).
(11) Kumar, S.; Giovannetti, G.; Brink, J. V. D.; Picozai, S. Theoretical Prediction of Multiferroicity in Double Perovskite Y_2NiMnO_6. *Phys. Rev. B* **2010**, *82*, 134429−134434.
(12) Swaminathan, V.; Pramana, S. S.; White, T. J.; Chen, L.; Chukka, R.; Ramanujan, R. V. Microwave Synthesis of Non-centrosymmetric $BaTiO_3$ Truncated Nanocubes for Charge Storage Applications. *ACS Appl. Mater. Interfaces* **2010**, *11*, 3037−3042.
(13) Su, J.; Zhang, J. T.; Lu, X. M.; Lu, C. J.; He, J.; Li, Q. C.; Zhou, J.; Zhu, J. S. Magnetic and Dielectric Properties of Metamagnetic $TbCo_{0.5}Mn_{0.5}O_{3.07}$ Ceramics. *J. Mater. Sci.* **2014**, *49*, 3681−3686.
(14) Mouallem-Bhout, M.; Roisnel, T.; Bouée, F.; André, G.; Moure, C.; Peña, O. Neutron Diffraction Evidence for a Cationic Order in the $REMn_{0.5}Ni_{0.5}O_3$ (RE = La, Nd) and $YMn_{0.5}Co_{0.5}O_3$ Perovskites. *Prog. Solid State Chem.* **2007**, *35*, 257−264.
(15) Kovalev, L. V.; Yarmolich, M. V.; Petrova, M. L.; Ustarroz, J.; Terryn, H. A.; Kalanda, N. A.; Zheludkevich, M. L. V. Double Perovskite Sr_2FeMoO_6 Films Prepared by Electrophoretic Deposition. *ACS Appl. Mater. Interfaces* **2014**, *6*, 19201−19206.

DOI: 10.1021/acsami.5b00911
ACS Appl. Mater. Interfaces 2015, 7, 13260−13265

(16) Khomchenko, V. A.; Troyanchuk, I. O.; Sazonov, A. P.; Sikolenko, V. V.; Szymczak, H.; Szymczak, R. Metamagnetic Behaviour in $TbCo_{0.5}Mn_{0.5}O_{3.06}$ Perovskite. *J. Phys.: Condens. Matter.* **2006**, *18*, 9541−9548.
(17) Krivanek, O. L.; Chisholm, M. F.; Nicolosi, V.; Pennycook, T. J.; Corbin, C. J.; Delby, N.; Murfitt, M. F.; Own, C. S.; Szilagyi, Z. S.; Oxley, M. P.; Pantelides, S. T.; Pennycook, S. J. Atom-by-Atom Spectroscopy at Graphene Edge. *Nature* **2010**, *464*, 571−574.
(18) Bosman, M.; Keast, V. J.; Garcia-Munoz, J. L.; D'Alfonso, A. J.; Findlay, S. D.; Allen, L. J. Two-Dimensional Mapping of Chemical Information at Atomic Resolution. *Phys. Rev. Lett.* **2007**, *99*, 086102−086105.
(19) Muller, D. A.; Kourkoutis, L. F.; Murfitt, M.; Song, J. H.; Hwang, H. Y.; Silcox, J.; Dellby, N.; Krivanek, O. L. Atomic Scale Chemical Imaging of Composition and Bonding by Aberration Corrected Microscopy. *Science* **2008**, *319*, 1073−1076.
(20) Bocher, L.; Popova, E.; Nolan, M.; Gloter, A.; Chikoidze, E.; March, K.; Warot-Fonrose, B.; Berini, B.; Stéphan, O.; Keller, N.; Dumont, Y. Direct Evidence of Fe^{2+}−Fe^{3+} Charge Ordering in the Ferrimagnetic Hematite−Ilmenite $Fe_{1.35}Ti_{0.65}O_{3-\delta}$ Thin Films. *Phys. Rev. Lett.* **2013**, *111*, 167202−167207.
(21) Brunner, E. W.; Jurewicz, I.; Heister, E.; Fahimi, A.; Chiara, B.; Sear, R. P.; Donovan, P. J.; Dalton, A. B. Growth and Proliferation of Human Embryonic Stem Cells on Fully Synthetic Scaffolds Based on Carbon Nanotubes. *ACS Appl. Mater. Interfaces* **2014**, *6*, 2598−2603.
(22) Luo, S. J.; Wang, K. F.; Li, S. Z.; Dong, X. W.; Yan, Z. B.; Cai, H. L.; Liu, J.-M. Enhanced Ferromagnetism and Ferroelectricity in Multiferroic $CuCr_{1-x}Ni_xO_2$. *Appl. Phys. Lett.* **2009**, *94*, 172504−172507.
(23) Su, J.; Lu, X. M.; Zhang, C.; Zhang, J. T.; Sun, H.; Ju, C. C.; Wang, Z. J.; Min, K. L.; Huang, F. Z.; Zhu, J. S. Study on Dielectric and Magnetic Properties of $Ho_3Fe_5O_{12}$ Ceramics. *Phys. B* **2012**, *407*, 485−488.
(24) Toby, B. H. EXPGUI, A Graphical User Interface for GSAS. *J. Appl. Crystallogr.* **2001**, *34*, 210−213.
(25) Carver, J. C.; Schweitzer, G. K.; Carlson, T. A. Use of X-ray Photoelectron Spectroscopy to Study Bonding in Chromium, Manganese, Iron, and Cobalt Compounds. *J. Chem. Phys.* **1972**, *57*, 973−982.
(26) Zhang, C. Y.; Zhang, T. S.; Ge, L.; Wang, S.; Yuan, H. M.; Feng, S. H. Hydrothermal Synthesis and Multiferroic Prpoperties of Y_2NiMnO_6. *RCS Adv.* **2014**, *4*, 5069−5074.
(27) Tan, H.; Turner, S.; Yücelen, E.; Verbeek, J. Temdeloo. 2D Atomic Mapping of Oxidation States in Transition Metal Oxides by Scanning Transmission Electron Microscopy Energy-Loss Spectroscopy. *Phys. Rev. Lett.* **2011**, *107*, 107602−107605.
(28) Azuma, M.; Takata, K.; Saita, T.; Ishiwata, S.; Shimakawa, Y.; Takano, M. Designed Ferromagnetic, Ferroelectric Bi_2NiMnO_6. *J. Am. Chem. Soc.* **2005**, *127*, 8889−8892.
(29) Yáñez-Vilar, S.; Mun, E. D.; Zapf, V. S.; Ueland, B. G.; Gardner, J. S.; Thompson, J. D.; Singleton, J.; Sánchez-Andújar, M.; Mira, J.; Bishop, N.; Seúarís-Rodríguez, M. A.; Batista, C. D. Multiferroic Behavior in the Double Perovskite Lu_2MnCoO_6. *Phys. Rev. B* **2011**, *84*, 134427−134434.
(30) Maiti, R. P.; Dutta, S.; Mukherjee, M.; Mitra, M. K.; Chakravorty, D. Magnetic and Dielectric Properties of Sol−Gel Derived Nanoparticles of Double Perovskite. *J. Appl. Phys.* **2012**, *112*, 044311.
(31) Lin, L.; Guo, Y. J.; Xie, Y. L.; Dong, S.; Yan, Z. B.; Liu, J.-M. Spin Frustration Destruction and Ferroelectricity Modulation in Ca_3CoMnO_6: Effects of Mn Deficiency. *J. Appl. Phys.* **2012**, *111*, 07D901−07D903.
(32) Ding, P.; Li, L.; Guo, Y. J.; He, Q. Y.; Gao, X. S.; Liu, J.-M. Influence of Co:Mn Ratio on Multiferroicity of $Ca_3Co_{2-x}Mn_xO_6$ Around $x \sim 1$. *Appl. Phys. Lett.* **2010**, *97*, 032901−032903.

DOI: 10.1021/acsami.5b00911
ACS Appl. Mater. Interfaces 2015, 7, 13260−13265